ACS APPLIED MATERIALS & INTERFACES
Research Article
www.acsami.org

# $BiVO_4/CeO_2$ Nanocomposites with High Visible-Light-Induced Photocatalytic Activity

Natda Wetchakun,*[,†] Saranyoo Chaiwichain,[†] Burapat Inceesungvorn,[‡] Kanlaya Pingmuang,[§] Sukon Phanichphant,[§] Andrew I. Minett,[⊥] and Jun Chen*[,#]

[†]Department of Physics and Materials Science, [‡]Materials Science Research Centre, and [§]Department of Chemistry, Faculty of Science, Chiang Mai University, Chiang Mai 50200, Thailand

[⊥]Laboratory for Sustainable Technology, School of Chemical and Biomolecular Engineering, University of Sydney, Sydney, Australia

[#]Intelligent Polymer Research Institute, ARC Centre of Excellent for Electromaterials Science, Australian Institute of Innovative Materials, University of Wollongong, Wollongong, NSW 2522 Australia

*Supporting Information*

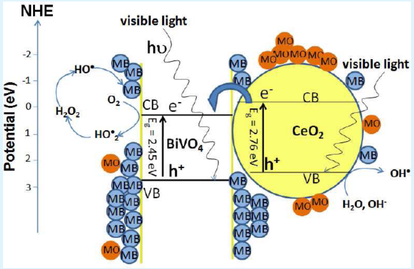

**ABSTRACT:** Preparation of bismuth vanadate and cerium dioxide ($BiVO_4/CeO_2$) nanocomposites as visible-light photocatalysts was successfully obtained by coupling a homogeneous precipitation method with hydrothermal techniques. The $BiVO_4/CeO_2$ nanocomposites with different mole ratios were synthesized and characterized by X-ray diffraction (XRD), Raman spectroscopy, and transmission electron microscopy (TEM). Absorption range and band gap energy, which are responsible for the observed photocatalyst behavior, were investigated by UV−vis diffuse reflectance (UV−vis DR) spectroscopy. Photocatalytic activities of the prepared samples were examined by studying the degradation of model dyes Methylene Blue, Methyl Orange, and a mixture of Methylene Blue and Methyl Orange solutions under visible-light irradiation (>400 nm). Results clearly show that the $BiVO_4/CeO_2$ nanocomposite in a 0.6:0.4 mol ratio exhibited the highest photocatalytic activity in dye wastewater treatment.

**KEYWORDS:** *$BiVO_4$, $CeO_2$, degradation, nanocomposites, photocatalytic activity, visible light*

## INTRODUCTION

The application of heterogeneous semiconductor photocatalysts in water cleaning and environmental remediation has recently attracted considerable attention because of their successful utilization of solar energy which is a natural abundant energy source.[1] Of all semiconductor photocatalysts employed in water purification, $TiO_2$ with a band gap energy of 3.2 eV was found to exhibit high photocatalytic activity under UV light irradiation. Apart from the most commonly used $TiO_2$ catalyst, cubic fluorite cerium dioxide ($CeO_2$), a semiconductor with a band gap energy similar to that of $TiO_2$,[2] also shows promising photocatalytic activity for the degradation of various organic dye pollutants such as Methylene Blue (MB), Methyl Orange (MO) and C.I. Reactive Black 5 (RB5).[3,4] $CeO_2$ has also successfully been employed in water splitting for $H_2$ production and phenol and chlorinated phenol photodegradation under UV illumination.[5,6] Although photocatalytic activity of $CeO_2$ has intensively been investigated, the broad band gap energy of this material limits its further application in the visible light region.[7] Therefore, recent effort has been devoted to narrowing the band gap energy of $CeO_2$ photocatalysts either by doping with metal/nonmetal elements or by forming heterojunctions between $CeO_2$ and other narrow band gap semiconductors in order to generate visible light-driven catalysts.[8,9]

By using coupled semiconductor photocatalysts, improved charge separation, increased charge carrier lifetime and thus enhanced photocatalytic activity due to high efficiency of the interfacial charge transfer from catalyst to adsorbed substrate can be obtained.[8−10] As a result, photocatalytic properties of $CeO_2$-based composite materials have been extensively explored. Hu and co-workers[8] investigated the catalytic performance of $Cu_2O/CeO_2$ heterojunction photocatalyst and found that the coupled semiconductor photocatalyst showed stronger visible light absorption capacity compared to pure $CeO_2$. The composite catalyst also exhibited 20% higher photocatalytic degradation of Acid Orange 7 (AO7) than that of pure $CeO_2$ under visible light illumination. An increased photoactivity of this composite catalyst was ascribed to the formation of p-n junctions, which are favorable for charge carrier separation. Photocatalytic degradation of Rhodamine B over $Bi_2O_3/CeO_2$ catalyst under visible-light irradiation was also evaluated by Li and Yan.[9] Therein, $Bi_2O_3/CeO_2$ in the 9:1 molar ratio gave maximum photodegradation activity and the Rhodamine B substrate was completely degraded within 8 h of irradiation. The enhancement of photocatalytic efficiency was believed to be due to an increased charge carrier lifetime obtained from the use of a composite photocatalyst. Li and co-workers[11] studied the photocatalytic degradation of Rhodamine B over ZnO/

**Received:** May 10, 2012
**Accepted:** June 29, 2012
**Published:** June 29, 2012

dx.doi.org/10.1021/am300812n | *ACS Appl. Mater. Interfaces* 2012, 4, 3718−3723

$CeO_2$ composite nanofibers prepared by an electrospinning technique and observed that the composite photocatalyst was able to completely degrade the dye substrate within 3 h whereas only 17.4% and 82.3% degradations were obtained in the case of pure $CeO_2$ and pure ZnO, respectively.

In our present study, we have investigated the photocatalytic efficiency of a $BiVO_4/CeO_2$ composite, in which $CeO_2$ was coupled with Bismuth Vanadate ($BiVO_4$) to form composites in different mole ratios. $BiVO_4$ was chosen as a sensitizer semiconductor due to its narrow band gap energy of 2.4 eV.[12,13] Pure $BiVO_4$ has previously been investigated for its photocatalytic properties as well as its application in water splitting and wastewater treatment.[14−16] However, to the best of our knowledge, the photocatalytic activity of $BiVO_4/CeO_2$ composite has not been reported. Therefore, the aim of this study is to elucidate the photocatalytic efficiency of this novel $BiVO_4/CeO_2$ composite material with an expectation to obtain a promising visible-light driven catalyst. The coupled semiconductor photocatalyst was successfully synthesized by the combination of the homogeneous precipitation and hydrothermal methods and its photocatalytic performance was evaluated via photodegradation of MB, MO, and a mixture of MB and MO solutions under visible-light irradiation.

## 2. EXPERIMENTAL SECTION

**2.1. Photocatalyst Synthesis.** $BiVO_4/CeO_2$ nanocomposite catalysts with different mole ratios between $BiVO_4$ and $CeO_2$ have been prepared by the combination of homogeneous precipitation and hydrothermal method. First, pure $CeO_2$ was synthesized by the homogeneous precipitation method using Cerium(III) nitrate hexahydrate ($Ce(NO_3)_3{\cdot}6H_2O$) as a cerium precursor. In a typical procedure, 10.91 g of $Ce(NO_3)_3{\cdot}6H_2O$ was dissolved in 100 mL of 80% v/v ethylene glycol solution. The solution was kept under constant stirring and heated at 50 °C until a homogeneous solution was obtained. After that, 25 mL of 3.0 M Ammonium hydroxide ($NH_4OH$) was slowly added into the above solution. The transparent solution immediately changed to a yellowish suspension. The suspension was kept under stirring at 50 °C for a further 24 h and the precipitate was finally collected by centrifugation, washed 3 times with deionized water and then dried at 80 °C for 24 h. The obtained powder was consequently calcined at 500 °C for 1 h. The as-synthesized $CeO_2$ powders were subsequently added to the preprepared mixture solution of Bismuth nitrate hexahydrate ($Bi(NO_3)_3{\cdot}6H_2O$) in nitric acid and Ammonium vanadate ($NH_4VO_3$) in ammonia solution (1:1 mol ratio) to form suspensions with different $BiVO_4$:$CeO_2$ mole ratios, 0.2:0.8, 0.4:0.6,0.6:0.4, and 0.8:0.2. The pH of the prepared suspension was adjusted to 7 by slowly adding 0.1 M of $NH_4OH$ solution. The suspension was then transferred into a Teflon-lined stainless steel autoclave and the hydrothermal reaction was carried out at 120 °C for 6 h. Finally, $BiVO_4/CeO_2$ composite was obtained by filtration and drying at 80 °C for 24 h. The as-synthesized composites were characterized and confirmed for the ratio of $BiVO_4$:$CeO_2$ via elemental analysis of Bi (related to $BiVO_4$) and Ce (related $CeO_2$). For control experiments, pure $BiVO_4$ photocatalyst was also prepared by the procedure described above.

**2.2. Characterization Studies.** The crystalline phases of pure $BiVO_4$, pure $CeO_2$ and $BiVO_4/CeO_2$ were determined by powder X-ray diffraction analysis (XRD, JEOL JDX-3530). The diffraction patterns were recorded in the range of $2\theta$ = 20 to 70° using Cu $K_\alpha$ radiation ($\lambda$ = 0.15406 nm) with a step scan of 0.5°/min. Raman spectra were measured at room temperature using a Jobin-Yvon T64000 triple-stage spectrograph with a spectral resolution of 2 $cm^{-1}$. A 632 nm He−Cd laser was used as the excitation source with an output power of 25 mW. Morphologies and microstructures of the as-prepared samples were examined by transmission electron microscopy (TEM, JEOL JEM-2010). UV−vis DR spectra of the photocatalyst particles were recorded at room temperature in the range of 300−700 nm using a Lambda 950 UV−vis spectrophotometer. The absorption spectra were obtained by analyzing the reflectance measurement with Kubelka−Munk (KM) emission function, $F(R_\infty)$. Optical band gap energy ($E_g$) can be determined from the plot between $E = 1240/\lambda_{\text{Absorp.Edge}}$ and $[F(R_\infty)h\upsilon]^{1/2}$ where E is the photonic energy in eV and $h\upsilon$ is the energy of an incident photon. Isoelectric point (IEP) of $BiVO_4$and $CeO_2$ particles was also examined by zetasizer nano instrument (ZS Malvern).

**2.3. Photocatalytic Activity for the Degradation of Dyes.** Visible light photocatalytic activities of $BiVO_4$, $CeO_2$, and $BiVO_4/CeO_2$ composite powders were evaluated through the decoloration of MB, MO, and the mixture of MB and MO solution with an initial dye concentration of $2 \times 10^{-5}$ M. Slurry batch reactor equipped with halogen lamp and a 400 nm cut off filter, providing a light intensity of 185 mW $cm^{-2}$, was used in this study. In a typical run, 0.05 g of photocatalyst was dispersed in 50 mL of Milli-Q water using ultrasonic probe for 30 min. The predetermined amount of organic dye was subsequently added into the catalyst suspension. After that, the suspension was stirred for 30 min in the dark to ensure adsorption/desorption equilibrium before light illumination. During the irradiation procedure, the reaction sample was collected at 20-min intervals and centrifuged to remove photocatalyst particles. The concentration of MB and/or MO substrates was then determined by measuring the absorbance at $\lambda_{max}$ 664.5 nm and $\lambda_{max}$ 463 nm, respectively, via UV−vis spectrophotometer (Shimadzu UV-1800).

## 3. RESULTS AND DISCUSSION

**3.1. XRD Analysis of $BiVO_4/CeO_2$ Nanocomposites.** Figure 1 shows the XRD patterns of novel $BiVO_4/CeO_2$ nanocomposites in comparison with those of pure $BiVO_4$ and pure $CeO_2$. The diffraction peaks of pure $BiVO_4$ at $2\theta$ of 28.8°, 30.55°, 34.5°, 35.2°, 39.8°, and 42.5° were respectively indexed as (112), (004), (200), (020), (211), and (015) planes of monoclinic $BiVO_4$ according to the Joint Committee Powder Diffraction Standards (JCPDS) file no. 75−1866. Although the diffraction peaks at $2\theta$ of 24.6° and 32.9° belong to the (200) and (112) planes of tetragonal $BiVO_4$ with JCPDS file no. 14−0133. Diffraction peaks of pure $CeO_2$ at $2\theta$ of 28.8°, 33.3°, 47.6°, and 56.4°can be indexed as the (111), (200), (220), and (311) planes of fluorite $CeO_2$ with JCPDS file no. 34−0394. The XRD patterns of $BiVO_4/CeO_2$ nanocomposites exhibited characteristic diffraction peaks of both $BiVO_4$ and $CeO_2$ crystalline phases. It can be seen from Figure 1 that, at low concentration of $BiVO_4$ (0.2 mol ratio), the diffraction pattern of the nanocomposite materials was quite similar to that of pure

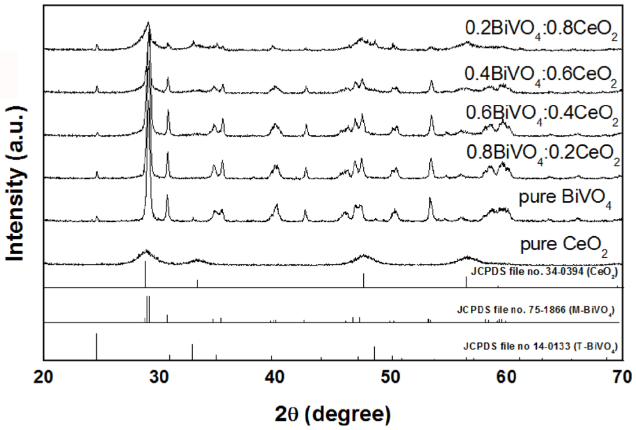

**Figure 1.** XRD patterns of pure $BiVO_4$, pure $CeO_2$, and $BiVO_4/CeO_2$ varying mole ratio; tetagonal $BiVO_4$ (T-$BiVO_4$) and monoclinic $BiVO_4$ (M-$BiVO_4$).

$CeO_2$. However, upon increasing the mole ratio of $BiVO_4$ in the nanocomposite sample, the diffraction pattern was more similar to that of pure $BiVO_4$. This is possibly due to the high crystallinity of the $BiVO_4$ phases, thus appearing as the dominant peaks in the XRD spectra of the nanocomposite samples. The XRD results also clearly indicated that $BiVO_4$ in the as-synthesized $BiVO_4/CeO_2$ composite presented in two crystalline phases, which are monoclinic and tetragonal structures. Calculation of the normalized ratios of relative intensities corresponding to these two different phases of $BiVO_4$, suggests that the monoclinic structure presents as a predominant phase (>90%) in the obtained $BiVO_4/CeO_2$ composite samples.

**3.2. Raman Spectra Measurement.** Raman spectroscopy provided further structural evidence as to the composition of the composites, as shown in Figure 2. The vibrational peaks at 121.96, 220.15, 322.32, 378.04, 720.96, and 831.14 $cm^{-1}$ observed from the pure $BiVO_4$ sample were in good agreement with those from the work of Gotić et al.[17] and Zhang et al.[18] The peaks at 720.96 and 831.14 $cm^{-1}$ were ascribed to asymmetric and symmetric V−O stretching modes, respectively. Although the peaks at 322.32 and 378.04 $cm^{-1}$ reflected the asymmetric and symmetric bending vibrations of $VO_4^{3-}$. Another two vibrational peaks at lower wavenumber (121.96 and 220.15 $cm^{-1}$) were assigned to external vibration modes. For the pure $CeO_2$ sample, only one main vibrational band at 463.78 $cm^{-1}$ is observed, because of the Ce−O bond vibration.[19] In the case of nanocomposite materials, characteristic Raman peaks for both $BiVO_4$ and $CeO_2$ were found. Interestingly, the composite spectra also clearly show a decreasing $CeO_2$ peak intensity when the mole ratio of $BiVO_4$ to $CeO_2$ is increased (the insert in Figure 2). This could be attributed to a lower coverage of $CeO_2$ on the $BiVO_4$ surface.

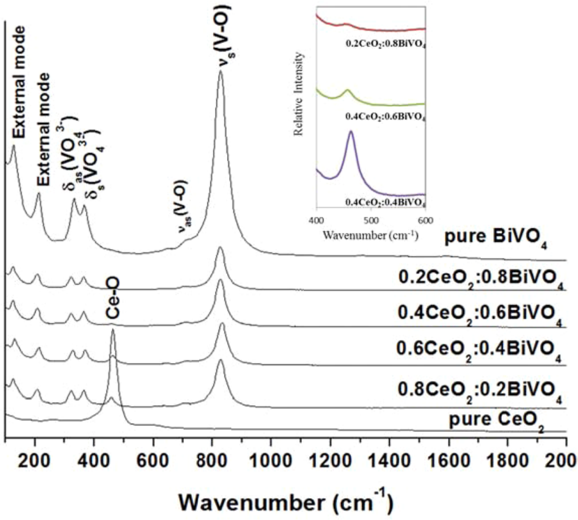

**Figure 2.** Raman spectra of all photocatalyst samples; and highlight of Ce−O responses for $0.2CeO_2{:}0.8BiVO_4$, $0.4CeO_2{:}0.6BiVO_4$, and $0.6CeO_2{:}0.4BiVO_4$ (the insert).

**3.3. Morphology Characterization.** The morphology of pure $CeO_2$ (Figure 3a) shows spherical-shaped nanoparticles with a diameter in the range of 5−10 nm, whereas pure $BiVO_4$ from TEM analysis (Figure 3b) was found to be rod-like particles with approximately 100 nm dimensions. The as-synthesized $BiVO_4/CeO_2$ composite via the modified coupling synthesis method (Figure 3c, d) clearly shows the presence of $CeO_2$ nanoparticles deposited onto the $BiVO_4$ surface. As shown in Figure 3d, it clearly shows two different crystal structures on the composite surface, which can be assigned to $CeO_2$ (left) and $BiVO_4$ (right), suggesting a high degree of crystallinity. This confirms that $BiVO_4/CeO_2$ nanocomposites were successfully prepared with $CeO_2$ nanoparticles covering the $BiVO_4$ surface.

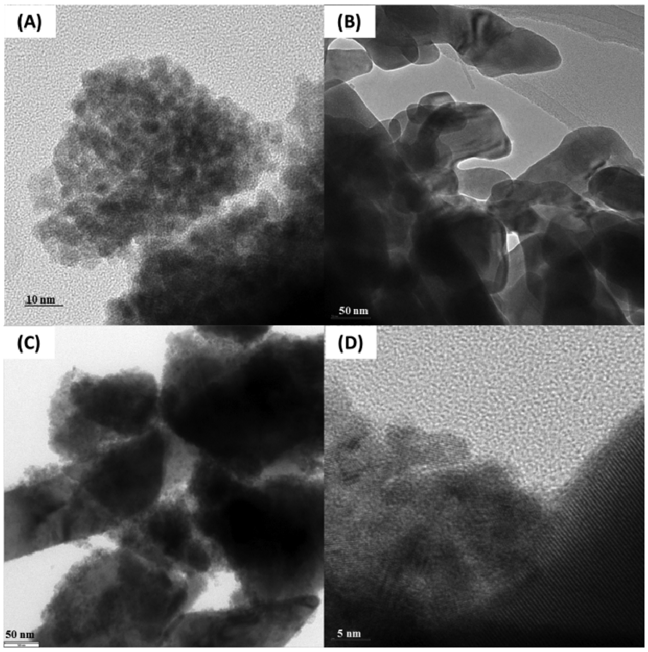

**Figure 3.** TEM images and electron diffraction patterns of (a) pure $CeO_2$, (b) pure $BiVO_4$, (c, d) $0.6BiVO_4{:}0.4CeO_2$ nanocomposites.

**3.4. UV−Vis Diffuse Reflectance Spectra and Band Gap Energy.** The UV−vis DR spectra of pure $BiVO_4$, pure $CeO_2$ and $BiVO_4/CeO_2$ composite are shown in Figure 4a. The optical band gap energy ($E_g$) can be determined from the plot between $E = 1240/\lambda_{\text{Absorp. Edge}}$ and $[F(R_\infty)h\upsilon]^{1/2}$ as shown in Figure 4b. Pure $CeO_2$ has an absorption onset at 420 nm, which corresponds to a band gap energy of 2.76 eV. The absorption edge of the $BiVO_4/CeO_2$ nanocomposites show a shift toward the visible region upon loading of $BiVO_4$ onto the $CeO_2$. According to Figure 4b, the nanocomposites in all $BiVO_4{:}CeO_2$ mole ratios possessed similar band gap energy of approximately 2.46 eV which is lower than the band gap energy of both pure $BiVO_4$ (2.51 eV) and pure $CeO_2$ (2.76 eV). This observation is important, as it indicates that the $BiVO_4/CeO_2$ nanocomposites can be photoexcited to generate more electron−hole pairs under visible-light irradiation, which could result in higher photocatalytic performance.

**3.5. Photocatalytic Activity for Methylene Blue (MB) Degradation.** The photocatalytic activities of all three $BiVO_4$, $CeO_2$, $BiVO_4/CeO_2$ photocatalysts were evaluated by measuring the decoloration of MB under visible light irradiation (>400 nm). The concentrations ($C$) of MB and MO were determined from UV−vis absorption studies by using the Beer−Lambert law relation at the maximum wavelength ($\lambda_{max}$) of 664.5 and 463 nm, respectively. Variations of MB concentration ($C/C_0$) with visible-light irradiation time over different catalysts are presented in Figure 5a, respectively. As a comparison, direct photolysis of MB as well as the photocatalytic degradation over

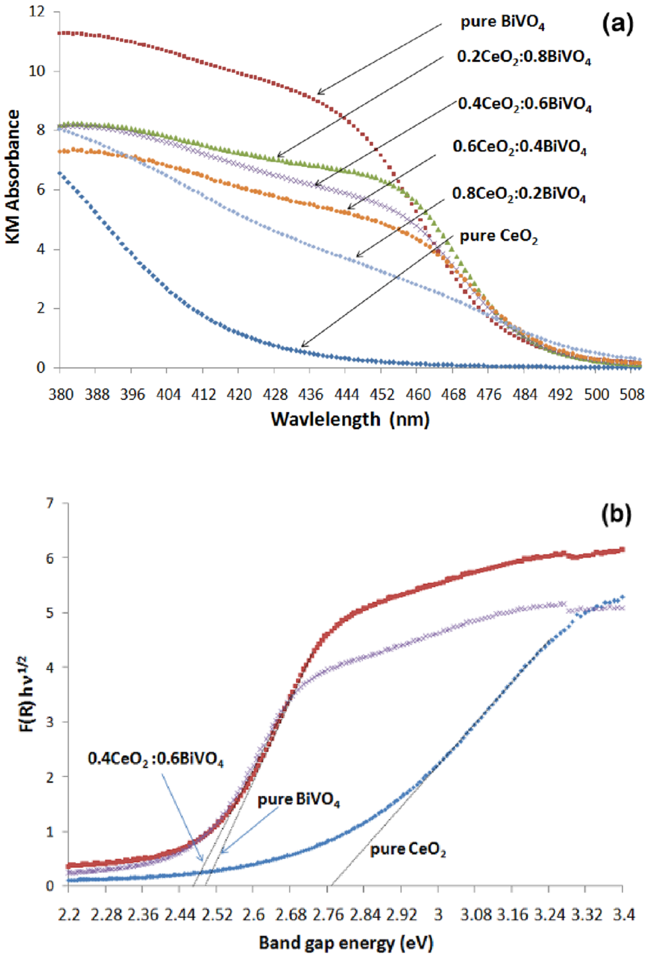

**Figure 4.** (a) KM absorbance plot and (b) band gap energy of pure $BiVO_4$, pure $CeO_2$, and different mole ratio of $BiVO_4/CeO_2$.

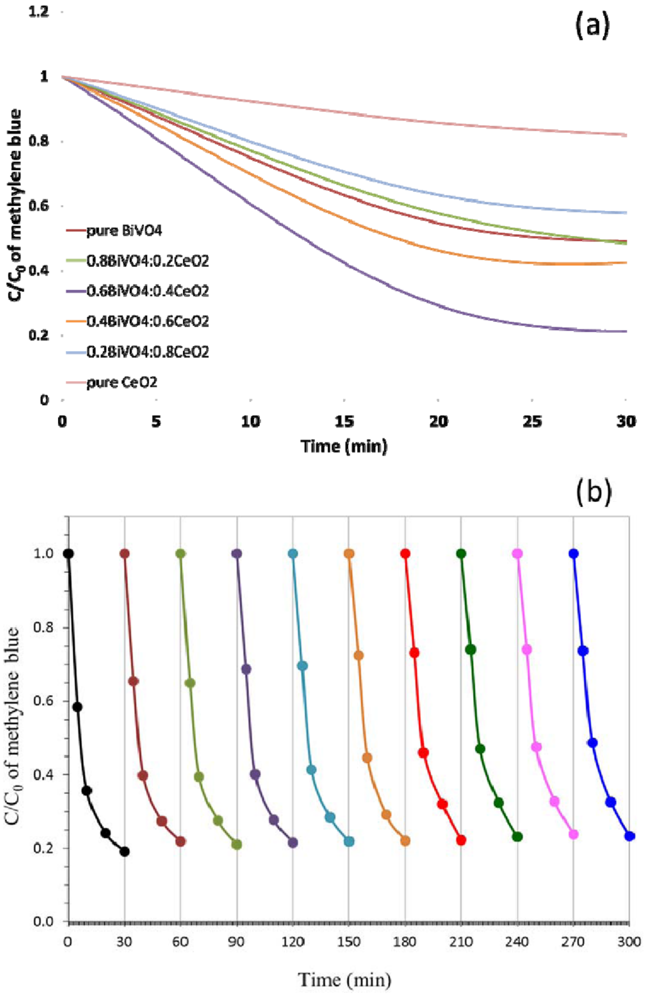

**Figure 5.** (a) Comparison of photodegradation efficiency of MB using all photocatalysts; (b) cycling runs of photodegradation of MB using $0.6BiVO_4$:$0.4CeO_2$ (initial concentration of MB 7.5 mg/L and catalyst loading 1 g/L).

pure $BiVO_4$ and $CeO_2$ were also performed under the identical conditions. All MB degradation curves of $C/C_0$ vs time displayed in Figure 5 are already normalized and calibrated from the photodegradation of MB in water in the absence of catalyst under identical conditions. As seen from Figure 5a, the mole ratio of $BiVO_4/CeO_2$ at 0.6:0.4 provided the highest photocatalytic activity where the highest MB degradation of 80% was obtained within 30 min of irradiation. It was found that lower or higher ratios than that of $0.6BiVO_4$:$0.4CeO_2$ lead to decreased photocatalytic performance. Stability of photocatalytic MB degradation using the selected $0.6BiVO_4/0.4CeO_2$ nanocomposite was also investigated as shown in Figure 5b. It was found that the $0.6BiVO_4/0.4CeO_2$ catalyst exhibited a highly stable photocatalytic performance toward MB degradation because no significant loss in activity was observed. It only displayed less than 10% deactivation after 10 cycles.

**3.6. Photocatalytic Activity for a Mixture of MB/MO Degradation.** This preferential degradation activity (MB) as a consequence of different adsorption ability between $BiVO_4$ and $CeO_2$ (in Figure 5) could be partially explained by the different surface charges characterized by zeta potential. The isoelectric point (no net charge) of $BiVO_4$ and $CeO_2$ were found at the pH of 4.56 and 7.33, respectively. This suggested that, under the photocatalytic conditions used in this study at pH 7, $BiVO_4$ and $CeO_2$ possessed negative and slightly positive charges on the surface, respectively. Because $BiVO_4$ has a net surface negative charge, the cationic methylene blue molecules would preferentially adsorb on $BiVO_4$ particles. On the contrary, $CeO_2$ particles possessing a slightly positive surface charge would preferably adsorb the anionic dye molecules, such as methyl orange, rather than MB. Therefore, a further preliminary study on the degradation of a mixture of dyes via adding MO into the preprepared MB solution was also investigated using selected $0.6BiVO_4/0.4CeO_2$ composite (as-synthesized) as well as physically mixed $0.6BiVO_4/0.4CeO_2$ as control. The reason for conducting a preliminary investigation utilizing dye mixtures is that real-world wastewater from industries would most likely contain more than one type of organic dyes.

Figure 6 illustrates the degradation efficiencies of the mixed solution of MO and MB over the $0.6BiVO_4/0.4CeO_2$ composite and mixed $0.6BiVO_4/0.4CeO_2$ catalysts. The results clearly confirm that both MB and MO dyes were preferentially degraded over as-synthesized $0.6BiVO_4/0.4CeO_2$ composite. This is possibly due to the strong interaction between $CeO_2$ and $BiVO_4$ as supported by the UV−vis DR spectra in Figure 4. In addition, the preliminary stability investigation of the $BiVO_4/CeO_2$ composite was also carried out for 5 cycles as shown in Figure 7. It was found that the composite catalyst exhibited stability toward both MB and MO degradations,

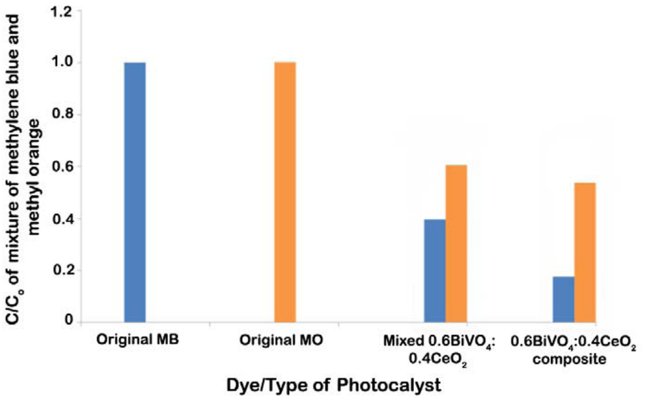

**Figure 6.** Comparison of photodegradation efficiency of a mixture of MB and MO solution using as-synthesized 0.6$BiVO_4$/0.4$CeO_2$ and mixed 0.6$BiVO_4$/0.4$CeO_2$ under identical conditions (initial concentration of both MB and MO 7.5 mg/L and catalyst loading 1 g/L).

because no significant loss in activity was observed after the second run.

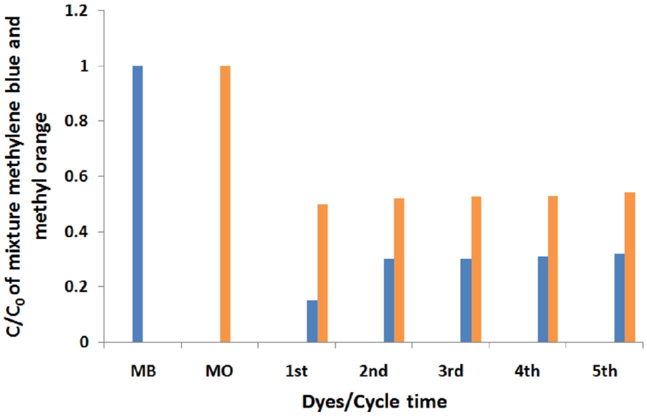

**Figure 7.** Cycling runs of photodegradation of the methylene blue and methyl orange mixture solution using 0.6$BiVO_4$:0.4$CeO_2$ (initial concentration of MO and MB 7.5 mg/L and catalyst loading 1 g/L).

An illustration of interparticle electron transfer behavior is proposed as shown in Figure 8. The band edge positions of the conduction band and valence band of a semiconductor can be determined using the equation:[2,13] $E^0_{CB} = \chi - E^C - 1/2E_g$, where $\chi$ is the absolute electronegativity of the semiconductor ($\chi$ is 5.56 eV[2] and 6.04 eV[13] for $CeO_2$ and $BiVO_4$, respectively). $E^C$ is the energy of free electrons on the hydrogen scale (4.5 eV) and $E_g$ is the band gap of the semiconductor. The calculated CB and VB of $BiVO_4$ were 0.28 and 2.78 eV, and of $CeO_2$ were −0.32 and 2.44 eV, respectively. According to Figure 6, when the $BiVO_4$/$CeO_2$ system is irradiated under visible light (>400 nm), both $CeO_2$ and $BiVO_4$ can be activated since the band gap energies of $CeO_2$ and $BiVO_4$ observed in this study were 2.76 and 2.51 eV. The excited electrons at the conduction band of $CeO_2$ crystallites are transferred to the conduction band of $BiVO_4$ crystallites. The electrons will then react with oxygen molecules to finally form hydroxyl radicals. These hydroxyl radicals will further oxidize the MB molecules that are preferentially adsorbed onto the $BiVO_4$ particles. However, in the case of the $CeO_2$, it is not so clear-cut. Although oxidizing species like hydroxyl radicals can indeed be formed on the $CeO_2$ surface, the availability of the MB species on, or near, the $CeO_2$ surface would be expected to be significantly less than that on the $BiVO_4$ surface. This is due to the fact that the $CeO_2$ particles possess a slightly positive surface charge (at pH 7), which would preferably adsorb anionic dye molecules, such as MO, rather than MB. Therefore, any MB degradation on the $CeO_2$ surface is quite low. As a result, more efficient charge-carrier separation, and thus improved photocatalytic activity could be achieved.[10,20]

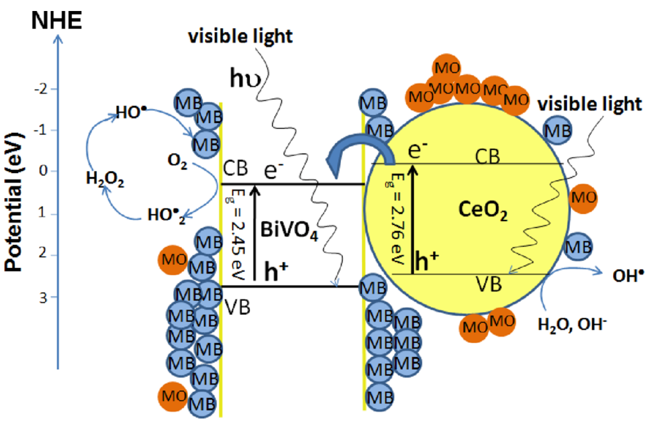

**Figure 8.** Possible photocatalytic mechanism for degradation of dyes over $BiVO_4$/$CeO_2$ nanocomposites under visible light irradiation (MB, methylene blue; MO, methyl orange).

## 4. CONCLUSIONS

Novel $BiVO_4$/$CeO_2$ nanocomposites with different mole ratios have been successfully prepared by homogeneous precipitation coupled with a hydrothermal method. These synthesis methods demonstrated good reproducibility and facilitated the production of high-purity products. The mole ratio of $BiVO_4$ to $CeO_2$ in the $BiVO_4$/$CeO_2$ composites was found to affect the degradation of dyes under visible light irradiation. The optimum mole ratio was found to be 0.6:0.4 ($BiVO_4$:$CeO_2$) showing the best photodegradation performance under visible light illumination. According to UV−vis DRS results, the absorption of $BiVO_4$/$CeO_2$ nanocomposites increased in the visible region (485−505 nm). Moreover, the low band gap energy of $BiVO_4$/$CeO_2$ nanocomposites also influenced the dyes degradation, and showed significant promise as a visible light photocatalyst for dye wastewater treatment. Further detailed studies to fully understand the mechanism are ongoing in our laboratories.

## ■ ASSOCIATED CONTENT

### Ⓢ Supporting Information

Variation of zeta potential with pH value of $CeO_2$ and $BiVO_4$, respectively. This material is available free of charge via Internet http://pubs.acs.org.

## ■ AUTHOR INFORMATION

### Corresponding Author

*E-mail: natda_we@yahoo.com (N.W.); junc@uow.edu.au (J.C.). Phone: +66-84-045-9424; +61 2 4221 3781. Fax: +66-53-892277;+61 2 4221 3781.

### Notes

The authors declare no competing financial interest.

## ACKNOWLEDGMENTS

The National Metal and Materials Technology Center (MTEC), the National Science and Technology Development Agency (NSTDA), Ministry of Science and Technology Grant (MT-B-53-CER-10-270-G); the National Research University Project under Thailand's Office of the Higher Education Commission, Materials Science Research Center; the Thailand Research Fund (TRF) and the Commission on Higher Education (CHE) Grant (MRG5480255); Thailand Graduate Institute of Science and Technology (TGIST), The National Science and Technology Development Agency (NSTDA) for Miss K.P.; Department of Chemistry and Department of Physics and Materials Science, Faculty of Science, Chiang Mai University; University of Wollongong International-Linkage Grant (UIC 2010/2011), for financial support; Mr. Victor Lo for HRTEM images of the particles at the University of Sydney's Centre for Microscopy & Microanalysis.

## REFERENCES

(1) Liotta, L. F.; Gruttadauria, M.; Carlo, G. D.; Perrini, G.; Librando, V. *J. Hazard. Mater.* **2009**, *162*, 588−606.

(2) Magesh, G.; Viswanathan, B.; Viswanath, R. P.; Varadarajan, T. K. *Indian J. Chem.* **2009**, *48A*, 480−488.

(3) Zhang, A.; Zhang, J. *Mater. Lett.* **2009**, *63*, 1939−1942.

(4) Song, S.; Xu, L.; He, Z.; Chen, J. *Environ. Sci. Technol.* **2007**, *41*, 5846−5853.

(5) Chung, K.-H.; Park, D.-C. *Catal. Today* **1996**, *30*, 157−162.

(6) Valente, J. S.; Tzomoantzi, F.; Prince, J. *Appl. Catal., B* **2011**, *102*, 276−285.

(7) Li, H.; Liua, G.; Duana, X. *Mater. Chem. Phys.* **2009**, *115*, 9−13.

(8) Hu, S.; Zhou, F.; Wang, L.; Zhang, J. *Catal. Commun.* **2011**, *12*, 794−797.

(9) Li, L.; Yan, B. *J. Non-Cryst. Solids* **2009**, *355*, 776−779.

(10) Liu, R.; Ye, H.; Xiong, X.; Liu, H. *Mater. Chem. Phys.* **2010**, *121*, 432−439.

(11) Li, C.; Chen, R.; Zhang, X.; Shu, S.; Xiong, J.; Zheng, Y.; Dong, W. *Mater. Lett.* **2011**, *65*, 1327−1330.

(12) Chatchai, P.; Murakami, Y.; Kishioka, S.-Y; Nosaka, A. Y.; Nosaka, Y. *Electrochimi. Acta* **2009**, *54*, 1147−1152.

(13) Jiang, H.-Q.; Endo, H.; Natori, H.; Nagai, M.; Kobayashi, K. *Mater. Res. Bull.* **2009**, *44*, 700−706.

(14) Ge, L. *Mater. Chem. Phys.* **2008**, *107*, 465−470.

(15) Zhou, Y.; Vuille, K.; Heel, A.; Probst, B.; Kontic, R.; Patzke, G. *Appl. Catal., A* **2010**, *375*, 140−184.

(16) Ge, L. *J. Mol. Catal. A: Chem.* **2008**, *282*, 62−66.

(17) Gotić, M.; Musić, S.; Ivanda, M.; Śoufekand, M.; Popović, S. *J. Mol. Struct.* **2005**, *744−747*, 535−540.

(18) Zhang, A.; Zhang, J.; Cui, N.; Tie, X.; An, Y.; Li, L. *J. Mol. Catal. A: Chem.* **2009**, *304*, 28−32.

(19) Kostić, R.; Aškrabić, S.; Dohčević, Z.; Popović, Z. V. *Appl. Phys. A: Mater.* **2008**, *90*, 679−683.

(20) Jiang, H.; Nagai, M.; Kobayashi, K. *J. Alloys Compd.* **2009**, *479*, 821−827.